Pattern of perturbations from a coherent quantum inflationary horizon

Craig Hogan

University of Chicago, 5640 South Ellis Ave., Chicago, IL 60637 Fermi National
Acclerator Laboratory, Batavia, IL 60510, United States of America

Abstract

It is proposed that if quantum states of space-time are coherent on null surfaces,
holographic Planck-scale fluctuations of inflationary horizons dominate the for-
mation of primordial scalar curvature perturbations. It is shown that the reduc-
tion of quantum states on nearly-spherical emergent horizon surfaces around
each observer creates a distinctive pattern whose correlations in the angular
domain differ from the standard quantum theory of inflation. Causal constraints
are used in a semiclassical model to formulate candidate directional symme-
tries. It is suggested that this hypothesis could provide a physical explanation
for several well known anomalies measured in CMB anisotropy. New exact
symmetries are predicted, such as a vanishing temperature correlation function
at 90 degrees angular separation, that can be tested with current data.

Keywords: cosmic background radiation, inflation, holography, cosmic
perturbations

(Some figures may appear in colour only in the online journal)

1. Introduction

A standard cosmological model [1] is now supported by a considerable body of evidence, espe-
cially precise measurements of correlations in cosmic microwave background radiation (CMB)
[2–13]. The early evolution is generally described by slow-roll inflation [14–16], during which
the repulsive gravity of an exotic, metastable scalar inflation field vacuum drives an acceler-
ating expansion. Inflation shapes the structure of the universe on the largest scales—a large,
nearly-uniform, nearly-flat geometry, with nearly-scale-invariant primordial perturbations in
curvature that give rise to cosmic structure. In the standard picture, the cosmic perturbations
are created by quantum fluctuations of the inflation field vacuum, coupled by linearized gravity
to the classical background geometry.

It is possible that all the classical elements of this picture are essentially correct, but that
the quantum mechanical model is radically incomplete, because its approximations omit a

fundamental coherence of emergent quantum gravity on causal surfaces. Instead of linearized quantum fields, cosmic perturbations could be dominated by spatially-coherent holographic degrees of freedom of Planck scale quantum geometry. Such holographic or 'spooky' scenarios [17, 18] do not assume a pre-existing, determinate classical background metric; instead, the perturbations are associated with the noisy emergence of space and time from a quantum system. Some theoretical motivations for this approach are summarized in the appendix below.

Unlike the standard scenario based on quantized inflation field modes, holographic inflation posits that the inflationary horizon of every observer, defined as its past light cone at the end of inflation, is a coherent nonlocal quantum object, like a whole atom. A similar hypothesis has recently been applied to the horizon in some quantum models of black holes [19–23]. In this picture, the quantum state of the horizon is a superposition of slightly deformed horizon surfaces, whose deformations are coherent at large angular separations. The cosmic time at which decoherence occurs at a given comoving position depends on the observer. Spatial projections and correlations of geometrical quantum states 'collapse' onto the nearly-spherical horizons instead of spatially infinite plane wave modes, so that primordial perturbations are laid down coherently, with nonlocal quantum correlations, on a nearly-spherical horizon in all directions.

The magnitude of the holographic perturbations depends only on H, the expansion rate during inflation in units of the Planck time $t_P \equiv \sqrt{\hbar G/c^5}$. Because of the coherence, the dimensionless perturbation power of scalar perturbations $\langle \Delta^2 \rangle \approx H t_P$ from Planck scale quantum gravity is much larger than the standard perturbations from quantum perturbations of inflation field modes on scale, $\langle \Delta^2 \rangle \approx (H t_P)^2 \epsilon^{-1}$, where ϵ denotes a slow-roll parameter of the inflation potential. Inflation therefore occurs at a lower H than in typical standard models, but because it also depends on a slowly varying H, the predicted primordial power spectrum of curvature in the holographic picture is indistinguishable from standard quantum inflation [18]: holographic inflation still produces perturbations with a nearly scale invariant, slightly tilted power spectrum. Post-inflation evolution is standard, so it preserves the precise match of standard cosmology to a host of measurements that depend only on the power spectrum, including CMB anisotropy spectra and measurements of cosmic large structure over a large range of scales.

The most distinctive observable relics of a coherent horizon [18] are new correlations in the initial phase and direction of classical curvature perturbations. It is proposed here that directly measurable signatures of these holographic correlations may appear in specific properties of the pattern of CMB anisotropy in the angular domain. They take the form of precisely defined symmetries or constraints that generally do not occur in any particular realization in the standard picture, because of cosmic variance. Simple constraints from causal structure and rotational symmetry in the emergent system are used here to derive precisely defined candidate symmetries of correlations at large angular separations.

The properties of the pattern derived here are better motivated, and more concretely specified, than previously conjectured holographic correlations [24–26]. They could provide a unified physical explanation of some long-known, seemingly unrelated statistical anomalies in the CMB [4, 8, 13]. Moreover, they lead to new predictions for properties that have no particular significance in the standard picture: for example, the most robust new prediction here is that the angular correlation function of curvature should exactly vanish at 90 degree angular separation. Perturbations can also naturally be generated with significant anticorrelation at large angular separations, at a level unlikely to occur in the standard picture. These predictions can be used to implement new, sharply formulated statistical comparisons with the standard quantum model of inflation.
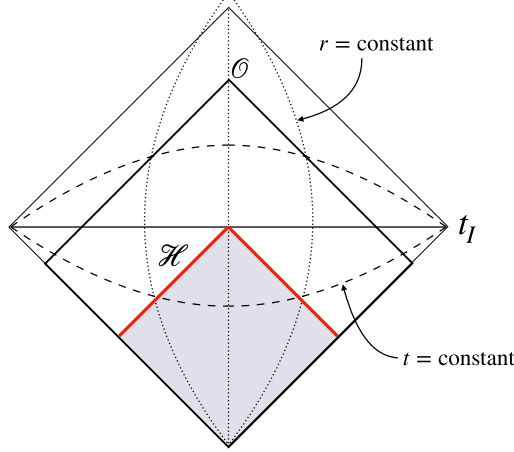
Figure 1. Causal structure of a classical inflationary universe, with two spatial dimensions suppressed. Vertical axis represents the world line of an observer $\mathcal{O}$, horizontal axis represents the end of inflation t_I, and left and right halves represent antipodal spatial directions. The horizon $\mathcal{H}$ forms the outer boundary of causal diamonds that end on $\mathcal{O}$ before t_I. Dashed lines represent spatial hypersurfaces of constant cosmic time t, and dotted lines are world lines of constant comoving position r. In standard inflation, the amplitude of a plane wave mode freezes out casually everywhere at the time when its wavelength matches the horizon, so quantum states of geometry collapse into eigenstates of wave modes on 3D spacelike hypersurfaces of constant t; in holographic inflation, geometrical states collapse on boundaries of causal diamonds defined by $\mathcal{H}$.

2. Holographic perturbations

2.1. Classical inflationary space-time

An unperturbed inflationary universe has a Friedmann–Lemâitre–Robertson–Walker metric, with space-time interval

$$\mathrm{d}s^2 = a^2(t)[c^2\mathrm{d}\eta^2 - \mathrm{d}\Sigma^2], \tag{1}$$

where t denotes proper cosmic time for any comoving observer, $\mathrm{d}\eta \equiv \mathrm{d}t/a(t)$ denotes a conformal time interval, and $a(t)$ denotes the cosmic scale factor, determined by the equations of motion. The spatial 3-metric in comoving coordinates is

$$\mathrm{d}\Sigma^2 = \mathrm{d}r^2 + r^2\mathrm{d}\Omega^2, \tag{2}$$

where the angular interval in standard polar notation is $\mathrm{d}\Omega^2 = \mathrm{d}\theta^2 + \sin^2\theta\mathrm{d}\phi^2$. Future and past light cones from an event are defined by a null path,

$$\mathrm{d}\Sigma = \pm c\mathrm{d}\eta. \tag{3}$$

Causal diagrams for an inflationary metric are shown in figures 1 and 2. The end of inflation t_I is taken to be the time when the expansion changes from accelerating, $\ddot{a} > 0$, to decelerating, $\ddot{a} < 0$. A causal diamond for an observer $\mathcal{O}$ with boundary at t_I corresponds to an interval with equal conformal time before and after t_I.

The inflationary horizon $\mathcal{H}$ is an inbound null surface that arrives at an observer $\mathcal{O}$ at the end of inflation. For our purpose, the exact choice of null surface (and t_I) does not matter; the
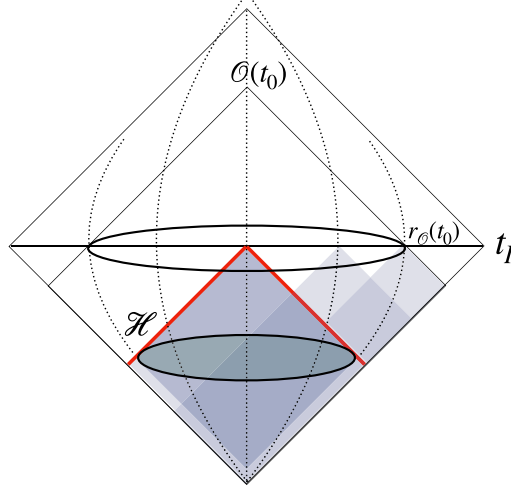
Figure 2. Formation of perturbations in holographic inflation. The geometry of the shaded region inside the horizon $\mathcal{H}$ has a coherent quantum relationship with the external region, and curvature perturbations in relation to $\mathcal{O}$ are matched to external classical values at the comoving location of its boundary. Each causal diamond surface centered on $\mathcal{O}$ is a 2-sphere of comoving radius $r_{\mathcal{O}}(t_0)$ with coherent perturbations relative to $\mathcal{O}$, indicated here by a filled oval. The relative potential of a comoving location is fixed when it exits $\mathcal{O}$'s inflationary horizon, when according to $\mathcal{O}$, it decoheres, or 'collapses' into a classical curvature perturbation. Other observers have different inflationary horizons (some of their causal diamonds are also shown as shaded regions) so the system as a whole, and in particular transverse positions on $\mathcal{H}$, remain in a superposition until t_I.

important thing is that $\mathcal{H}$ forms the future boundary of a series of causal diamonds of nearly constant area $4\pi(c/H)^2$ during the slow-roll phase.

2.2. Holographic inflation

To calculate quantum perturbations in the classical picture, the standard quantum model of inflation uses a straightforward extrapolation of field theory, including linearized quantum general relativity. The holographic hypothesis holds that this model is radically incomplete, because the linearized approximation to quantum gravity neglects the effects of nonlocal correlations in coherent geometrical states, including information that controls the spatial structure of quantum collapse and state reduction in transverse directions for each mode. Estimates of the physical effects of coherent quantum gravity in other contexts, such as flat space-time and black holes, are summarized below in the appendix.

With new holographic correlations of emergent quantum gravity, linearized general relativity no longer produces the most important scalar curvature fluctuations on the horizon scale, so it omits the dominant effect. The physical difference from the standard scenario is that quantum geometry collapses on coherent light cone states instead of linear plane wave states (figures 1–3). The relic classical curvature perturbations, relative to an observer's world line, originate on the horizon. During inflation, they are indeterminate inside the horizon, and some of their properties are frozen outside. Holographic correlations within the horizon create the new features of the relic pattern discussed here.
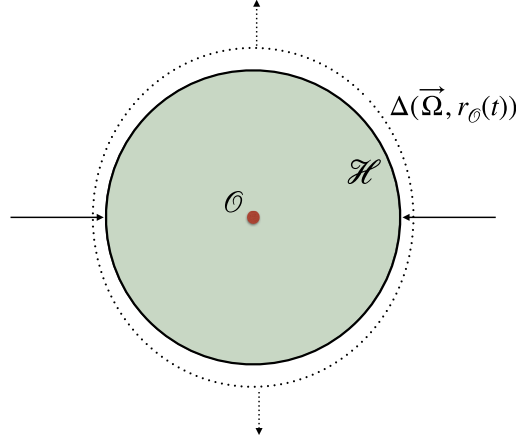
Figure 3. Two dimensions of a spatial hypersurface at a single cosmic time during infla-tion. The shaded region lies in the interior of the event horizon $\mathcal{H}$. Incoming arrows indicate directions of incoming null information on $\mathcal{H}$ coming from different directions in that frame. Dotted lines indicate the coherently perturbed outgoing comoving sphere that carries the reduced quantum state, which emerges as a conserved classical curva-ture perturbation $\Delta(\vec{\Omega}, r_{\mathcal{O}}(t))$. The distribution of Δ on this spherical comoving surface is correlated between all directions $\vec{\Omega}$, and matches the constraints of holographic causal symmetries on $\mathcal{H}$.

In a semiclassical model of holographic inflation [18], perturbations are due to quantum variations of holographic geometry in a nearly-uniform background that approximates stan-dard slow-roll inflation. The amplitude is dominated by the new geometrical uncertainty, so the model can omit the effect of inflation field perturbations. As usual, the initial power spectrum is nearly scale-invariant, with a small tilt that fits cosmological data with a simple effective poten-tial. However, new symmetries are generated on the horizon, associated with new holographic constraints.

In particular, collapse on the spherical horizon surface imprints large scale correlations on the initial state of classical perturbations in the directional domain. The phase correlations occur between directions around any observer, from the projection of the causal diamond states of the quantum system onto emergent classical wave vectors (figure 3). Consistency requires directionally coherent holographic correlations throughout causal diamonds. Phase correla-tions have a distinctive 3D structure different from any nongaussian field: coherent collapse occurs onto spherical horizons around every world line, rather than infinite plane waves [18]. The directional entanglements are most conspicuous on horizon scales similar to mode wave-length and at large angles, where the spherical curved surface of a horizon entangles different directions.

Features of holographic cosmology on subhorizon scales depend on the details of the funda-mental degrees of freedom. Ultimately, a radical conceptual reworking of quantum geometry from holographic effects should lead to a new mechanism of inflation, and may lead to new quantum effects that extrapolates to small scales, including estimated nonlinear effects from virtual black holes [17, 27]. In a comprehensive theory of quantum gravity the new geometri-cal states are connected with emergence of locality, inertial frames, angular momentum, and internal spin. The simpler semiclassical model adopted here and in reference [18], based on

linear perturbations of a classical background, is adequate to model the amplitude and some symmetries of new, nonlocal horizon-scale perturbations.

At the deeper level, a full theory of emergent gravity should account for the emergence of the cosmological background. Measurable geometrical relationships on emergent causal diamonds are invariant, but the distinction between perturbation and background is observer-dependent. For each even frozen perturbation mode, the part that projects onto the monopole harmonic on the sphere is absorbed into the background curvature for each observer; for each odd mode, the part that projects onto the dipole harmonic collapses the observer's world line to the local cosmic rest frame. An emergent background allows every observer to observe the same directional symmetries. The symmetries are the same over time for each observer, aside from changes in the fractionally small time variations from the slowly retreating horizon.

2.3. Semiclassical model of perturbations

The premise of holographic inflation is that nonlocal space-time indeterminacy creates coherent scalar curvature perturbations on horizons of the emergent inflationary metric. We adopt a semiclassical model where exotic geometrical correlations on the light cone $\mathcal{H}$ imprint correlations on the emergent curvature of comoving world lines as they pass through $\mathcal{H}$, as shown in figures 2 and 3.

Adopting standard conventions for linear perturbations [14–16], denote the invariant curvature perturbation [28] in comoving 3-space by $\Delta(\vec{r})$, and its spectral transform in comoving wavenumber space $\vec{k}$ on surfaces of constant cosmological time by

$$\tilde{\Delta}(\vec{k}) = \int \mathrm{d}\vec{r}\Delta(\vec{r})\mathrm{e}^{\mathrm{i}\vec{k}\cdot\vec{r}} = |\tilde{\Delta}(\vec{k})|\mathrm{e}^{\mathrm{i}\theta(\vec{k})}. \tag{4}$$

The following analysis concentrates on directional correlations, so perturbations will be described in the polar coordinates adopted for the metric, $\Delta(r, \theta, \phi)$.

Usually, quantum coherence is assigned and matched to the gravitational effect of plane-wave modes of amplitude $\tilde{\Delta}(\vec{k})$ on infinite spacelike hypersurfaces. In the holographic model, the relic curvature perturbations are matched to fluctuations of the quantum system projected on spherical causal diamond boundaries of the inflationary horizon $\mathcal{H}$. The fluctuations freeze in as differences of potential Δ from the observer when a comoving world line passes through the horizon.

As discussed in the appendix, the physical effects of coherent states [18], not accounted for in linearized gravity, can be estimated using standard classical relativity and quantum mechanics. The fractional fluctuation power of dimensionless perturbations on a coherent horizon of radius c/H is given by

$$\langle\Delta^2\rangle = Ht_\mathrm{p}, \tag{5}$$

where observed perturbations [2–12] have $\Delta^2 \sim 10^{-9}$. Perturbations that scale like equation (5) with slowly varying H produce a nearly-scale-invariant power spectrum indistinguishable from standard cosmology [17, 18], so they agree with standard spectral measurements of CMB anisotropy and cosmic structure for a suitable choice of inflationary potential. However, unlike the standard model, the coherent horizon has correlations among different spatial directions, and over a broad band of k.
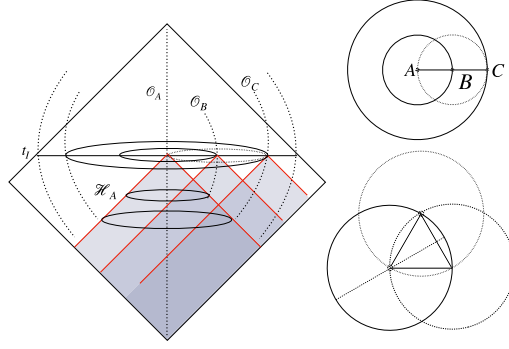
Figure 4. Spherical footprints of horizons for three world lines A, B, C, at particular comoving times in the frame of A. Slices of spheres are shown at the end of inflation at the right. Along any spatial line after this time, the sum of antipodal differences and sums must agree for any set of tangent spheres with centers on the line. Intersections of spheres centered on each other's boundaries requires symmetries in correlations of polar values with azimuthal averages. The special case of equal size spheres is associated with polar angles $\Theta = \pm 30°$, as shown at lower right.

2.4. Correlations on spherical horizon footprints

Even without a theory of quantum gravity, the semiclassical model allows application of principles governing coherent holographic emergence of a classical metric during inflation. The process should preserve statistical homogeneity, isotropy, and near-scale-invariance, so invariant scalar perturbations $\Delta(\vec{\Omega}, r_{\mathcal{O}}(t))$ freeze on nearly-spherical horizons defined by the homogeneous solution. In any observer's frame, the horizons around any world line define spherical 'footprints' at the end of inflation (figure 4), that intersect on circles. As usual in inflation, smaller spheres freeze later, with coherent displacements. Thus, smaller circles and angular positions also freeze later. Frozen values are coherent on circles for each sphere, so some statistical properties of Δ on equatorial circles freeze before those of smaller circles. The outcome at the end of inflation is classical and determinate, so the perturbations on the spheres are not independent: in particular, the linear sum of polar differences or sums of curvature along any line matches the total difference or sum.

Define the angular correlation function for angular separation Θ for any sphere,

$$C_\Delta(\Theta) \equiv \langle \Delta(\vec{\Omega}) \langle \Delta \rangle_{\Theta, \vec{\Omega}} \rangle_{\vec{\Omega}}, \tag{6}$$

where $\langle\rangle_{\Theta, \vec{\Omega}}$ denotes an azimuthal mean on a circle at a polar angle Θ about direction $\vec{\Omega}$. This quantity is measurable on any sphere after the end of inflation. The holographic spherical coherence places new constraints on $C_\Delta(\Theta)$; for example, we expect that frozen circles are correlated with frozen polar values only for intersections with smaller spheres that freeze out later. The intersections of equal-radius spheres centered on each other define particular angles where consistency requires exact, universal symmetries in the angular domain.

2.5. Candidate symmetries

We seek to test the hypothesis that the pattern of relic curvature $\Delta(r, \theta, \phi)$ is a coherent projection of a quantum state on the comoving sphere r when it leaves $\mathcal{H}$. The observed classical value
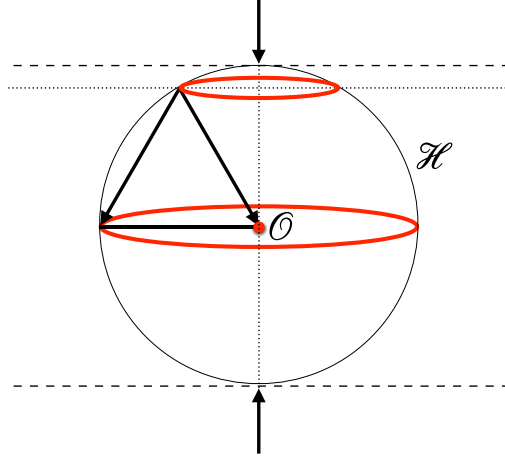
Figure 5. How azimuthal averages of emergent perturbations are constrained by causal symmetries of state reduction. The 2D spherical surface of $\mathcal{O}$'s horizon is shown in comoving 3-space at one time during inflation. Dashed lines represent the normal surfaces to a classical emergent polar direction around the observer, the tangent planes of incoming null surfaces on the horizon. Since this information from polar directions along any axis reaches the observer only at the end of inflation, it cannot be correlated with the mean perturbation on the equator, so the angular correlation function of curvature vanishes at $\Theta = 90°$. The equilateral triangle and dotted lines show a similar causal symmetry that affects global azimuthal averages of a collapsed causal diamond at $\Theta = 30°$: the polar information arrives at both the observer and the horizon equator at the end of inflation together with that from $\Theta = 30°$.

depends on the quantum phase of the state when it decoheres. The semiclassical model relates information flow in the classical world outside the horizon among events where it affects the phase of Δ when and where it decoheres, as a function of comoving position r, θ, ϕ. It allows us to identify candidate symmetries of correlations in curvature perturbations in θ, ϕ at a fixed r, derived from causal principles proposed to govern how emergence works. The candidate directional symmetries are based on the idea that emergent scalar curvature perturbations in different directions have nonlocal relationships determined by coherent states of a quantum system with some fundamental symmetries.

2.5.1. Azimuthal symmetries.   One consequence of emergent causality is that incoming phase information that determines polar values of potential along any given axis on the horizon only reaches the equatorial plane at the end of inflation, so it cannot affect the potential for points in that plane (see figure 5). As shown in the examples given in the appendix, the essential nature of coherent holographic uncertainty is that it is entirely transverse to the direction of propagation.

Uncorrelated incoming polar information produces the following *exact global equatorial symmetry* of relic curvature on each sphere around an observer:

$$\langle \Delta(\vec{\Omega}) \langle \Delta \rangle_{\perp \vec{\Omega}} \rangle_{\vec{\Omega}} = 0. \tag{7}$$

where $\langle \rangle_{\perp \vec{\Omega}}$ denotes the azimuthal mean on the great circle normal to direction $\vec{\Omega}$, and $\langle \rangle_{\vec{\Omega}}$ denotes an average over all directions $\vec{\Omega}$. Since by definition the point average vanishes,

$\langle\Delta(\vec{\Omega})\rangle_{\vec{\Omega}} = 0$, equation (7) follows if *the average* $\langle\Delta\rangle_{\perp\vec{\Omega}}$ *on each great circle is uncorrelated with the sum of its polar values*, $\Delta(\vec{\Omega}) + \Delta(-\vec{\Omega})$.

Such an exact equatorial symmetry would follow if there were exactly odd point parity, or if all great circles have vanishing mean ($\langle\Delta\rangle_{\perp\vec{\Omega}} = 0$). However, it does not require either of these to hold: it specifies an orthogonal rather than an antipodal relationship, and can hold exactly even if antisymmetry is not exact. It arises if *perturbations on orthogonal axes are always independently generated*. Equation (7) is equivalent to

$$C_\Delta(90°) = 0. \tag{8}$$

This symmetry does not apply in the standard scenario. In that case, equatorial azimuthal symmetry occurs only by chance, and only approximately: in a harmonic description, it requires a global 'conspiracy' of phases of even-parity modes. From this point of view, an exact equatorial azimuthal symmetry is the most simple and direct signature of emergent causal structure in holographic inflation.

As shown in figure 5, certain assumptions about how emergence works could also lead to an equilateral azimuthal symmetry. Consider the correlations of a polar value with points on its 30° azimuthal circle, both again determined by incoming phase information from the polar direction. Data from any polar point and from its 30° circle on the same sphere reach both the observer and the equator at the end of inflation. If the azimuthal mean is independent of its polar value, the global mean vanishes, so

$$C_\Delta(30°) = 0. \tag{9}$$

In a multipole expansion, a $C_\Delta(30°) = 0$ symmetry constrains odd as well as even spherical harmonics. In particular, a nonzero dipole contributes $C_\Delta(30°) \neq 0$: thus, for $C_\Delta(30°) = 0$ to appear on a dipole-subtracted sky, it must apply in the frame of an observer where the dipole vanishes. For this to occur independent of the cosmic rest frame, the intrinsic dipole, as viewed in the local matter rest frame, should itself vanish due a new symmetry that governs how the cosmic comoving frame emerges from a quantum system. The complementary azimuthal mean at $\Theta = 180° - 30° = 150°$ could be small but nonzero, depending on the origin of the local cosmic rest frame and global parity violation.

2.5.2. Constant variance on great circles. The global equatorial symmetry still allows mean values of Δ on great circles to vary according to random incoming polar information associated with each axis. A separate symmetry may be associated with nonlocal correlations of variance normal to each axis. It is possible that *the variance on great circles is a constant*, that is, it depends only on basic physics, rather than being a random variable.

This symmetry appears in a toy model described in the appendix. In (equation (38)), the commutator on the left-hand side that is responsible for the exotic quantum fluctuation has projected directional components orthogonal to the components on the right-hand side, related by the antisymmetric tensor ϵ_{ijk}, and leads to an uncertainty, equation (46). Thus, an eigenstate with $\delta\tau_3 = 0$ has an irreducible uncertainty in the sum of orthogonal components, $\langle\delta\tau_1^2 + \delta\tau_2^2\rangle$.

A similar symmetry applied to curvature during inflation would relate perturbation power in orthogonal directions. A possible consequence is that a directional average in the plane normal to any direction, say 3, obeys the same relation:

$$\langle\Delta^2\rangle_{\perp 3} = \langle\delta\tau_1^2 + \delta\tau_2^2\rangle/\tau^2 \geqslant \langle\Delta^2\rangle. \tag{10}$$

Suppose that cosmology preserves the symmetry of statistical isotropy, that is, statistical quantities are independent of direction. In order for equation (10) to hold for any direction in a single statistically isotropic distribution, the bound must saturate in all directions: if any direction were to exceed the overall average, another direction would need to have less than the lower bound. This leads to a symmetry of the azimuthal average variance:

$$\langle\Delta_\perp^2\rangle_\phi \equiv \int \mathrm{d}\phi'[\Delta(\phi', \theta' = \pi/2)]^2 = \langle\Delta^2\rangle, \tag{11}$$

for any orientation of polar coordinates (θ', ϕ'). That is, *the variance of curvature perturbations on any great circle is equal to the variance for the whole sky.*

The symmetry represented by equation (11) does not hold for random-phase noise in standard quantum inflation. It arises from the rotational symmetry of the quantum system, and the holographic absence of one independent rotational degree of freedom. Thus, it can be used to differentiate the distribution from the random Gaussian noise predicted in the standard model.

As usual, there is a zero mean variation averaged over all directions $\vec{\Omega}$,

$$\langle\Delta\rangle_{\vec{\Omega}} \equiv \iint \mathrm{d}\phi\mathrm{d}\theta \, \sin(\theta)\Delta(\phi, \theta) = 0, \tag{12}$$

so Δ can be decomposed into a linear sum of spherical harmonic components Y_ℓ^m. To satisfy the symmetry of great circle variance (equation (11)) they must have a coherent relationship that appears as a conspiracy of alignments and amplitudes. It is useful to illustrate with an example that uses a few low order spherical harmonics: octopole ($\ell = 3$), quadrupole ($\ell = 2$), and dipole ($\ell = 1$).

Suppose there is a dipole aligned along the z axis, with $\Delta_1 \propto \cos\theta$. It represents the intrinsic dipole of curvature in the polar direction, as viewed in the local cosmic rest frame. By itself, it obeys equation (11) for all great circles that pass through the pole, with normal directions in the x, y plane.

For the dipole alone, the variance on the equator $\theta = \pi/2$ vanishes so it does not satisfy equation (11). The other multipole moments must organize around this direction to have perturbations satisfying equation (11) in all directions. The fit improves if we add to the dipole a precisely aligned sectoral octopole ($\ell = |m| = 3$), with angular dependence $\Delta_3 \propto \mathrm{e}^{3i\phi} \sin^3\theta$, and a precisely aligned sectoral quadrupole ($\ell = |m| = 2$), with angular dependence $\Delta_2 \propto \mathrm{e}^{2i\phi} \sin^2\theta$. The dipole variance vanishes along the equator, while the octopole and quadrupole variances are maximized for an equatorial great circle. To create a pattern consistent with equation (11) in all directions requires correlations and alignments of higher multipoles, although the symmetry could apply over only a limited range of ℓ, depending on the angular coherence scale of correlations. Some manifestations of multipole alignment in the CMB are outlined below.

2.5.3. Antipodal anticorrelation and parity violation. The inflationary horizon could also display antipodal anticorrelation, a tendency of opposite points in the sky to have opposite signs. It occurs in quantum models of eternal black hole horizons [19–21], where antipodes on the horizon are actually identified, and time-reversed conjugate particle states are entangled at opposite spatial poles, even on macroscopic scales. In flat space-time, a toy model of quantum nonlocality (see the appendix below) derives point-parity antisymmetry directly from the Dirac light cone structure (equation (33)), which carries over into geometrical operators:

$$\hat{\tau}(x_\kappa) = -\hat{\tau}(-x_\kappa). \tag{13}$$

In our model of emergent inflation, the antipodal outgoing states of geometry on the horizon become antipodal curvature perturbations of the emergent metric. As discussed above, antipodal relationships are entangled with the emergence of local cosmic rest frame.

In standard inflation, any measured asymmetry in antipodal perturbation power is entirely due to 'cosmic variance' from the zero expected value of the ensemble. In the range of possible realizations, the bulk of the point-parity antisymmetry (or symmetry) is almost always contributed by a small number of harmonic modes on large angular scales, especially the intrinsic dipole and quadrupole.

In the holographic model, as in black holes, a coherent holographic horizon can provide a global constraint on even and odd parity relationships between opposite points in the sky for any realization. Indeed there may be no cosmic variance in the ratio of odd to even perturbation power; its value may be set by underlying asymmetric physics. In general, violation is not confined to low-ℓ modes.

To start with, consider the extreme case: frozen metric perturbations with exact antisymmetry similar to eternal black holes, so that the curvature in direction $\vec{\Omega}$ satisfies

$$\Delta(\vec{\Omega}) = -\Delta(-\vec{\Omega}), \tag{14}$$

an exactly odd point parity of perturbations. Microscopic spookiness is manifested macroscopically: points in opposite directions 'know about each other' like nearby ones do. Unlike the standard picture, *spooky correlation does not separate scales: it applies to fine-grain angular detail* (*that is*, *high resolution $\ell \gg 1$*), *even at large angular separation*. In this extreme example, the all-sky distribution has an antipodal variance equal and opposite to the single-point variance:

$$\langle \Delta(\vec{\Omega}) \Delta(-\vec{\Omega}) \rangle = -\langle \Delta^2 \rangle. \tag{15}$$

We should allow for the possibility of a less extreme imbalance of odd and even perturbations. In cosmology, as in a realistic time-asymmetric black hole, an exact antipodal antisymmetry can be broken by a background system that is not in a time-symmetric equilibrium or ground state. The exact antipodal antisymmetry of flat-space-time may not apply for inflationary perturbations, since the classical inflationary background breaks the time-displacement and boost symmetries of classical relativity, and the vacuum matter fields that couple to gravity also in general violate parity. The magnitude of time-direction symmetry breaking is related to how much the inflationary solution departs from that of the maximally symmetric de Sitter inflationary solution. One direct measure of time asymmetry comes from the slight tilt of the power spectrum from exact scale invariance, measured [10, 11] to be $1 - n_S = 0.035 \pm 0.004$, which arises from the small fractional decrease in the expansion rate during each e-folding of inflation [18]. We adopt a cosmological symmetry breaking parameter $\mathcal{E} < 1$, so that equation (15) becomes

$$\langle \Delta(\vec{\Omega}) \Delta(-\vec{\Omega}) \rangle = -\langle \Delta^2 \rangle (1 - \mathcal{E}), \tag{16}$$

where the ratio of even to odd perturbation power is $\mathcal{E}$.

In general, $\mathcal{E}$ depends on angular wave number ℓ. The fine grain character of parity asymmetry is best revealed by harmonic analysis. An analysis of temperature anisotropy can be found for example in figure 25 of reference [13], where the value of $\mathcal{E}$ for temperature anisotropy at

each ℓ is denote by R_{TT}. It shows a detection of $\mathcal{E}_{\mathrm{T}} \approx 0.3$ at ℓ of order a few, and a significant detection of power asymmetry up to $\ell \approx 30$.

3. Patterns in CMB anisotropy

It is useful to define measures of symmetry that can be used for empirical tests based on CMB anisotropy. The symmetries of curvature lead to simple predictions that can be used as the basis for tests on large angular scales, $\Theta = \mathcal{O}(1)$. The most distinctive signature of exotic symmetries is that they constrain this large-angle pattern even at high resolution, $\ell \gg 1$.

On large angular scales, CMB temperature anisotropy is dominated by perturbations within a relatively thin sphere at the epoch of last scattering, with some secondary effects from the intervening volume [29–31]. The direct effect of scalar perturbations on anisotropy is described by the Sachs–Wolfe approximation [29]; in this approximation, the pattern of δT preserves the pattern (and symmetries) of Δ. However, the fine-grained temperature distribution for harmonics $\ell \gg 1$ is significantly affected by Doppler motions, and these must be included in tests of precise symmetries, even at large angular separation, $\Theta \sim \mathcal{O}(1)$. Because the pattern of Doppler anisotropy for each 3D wave vector differs from the scalar pattern, a linear algorithm may be used to reconstruct the pattern of the primordial potential from measurements of temperature and/or polarization [32, 33], although this has not yet been done for an all-sky CMB map.

3.1. Symmetries of the correlation function

The two-point correlation function defined above (equation (6)) can also be written in terms of an empirical estimator

$$C_{\Delta}(\Theta) = \langle \Delta_a \Delta_b \rangle_{\angle ab = \Theta}, \tag{17}$$

an all-sky average over all pairs of points a, b at angular separation $\angle ab = \Theta$. Relics of primordial symmetries on the inflationary horizon survive in $\Delta(\theta, \phi)$ at last scattering, and can be reconstructed from measurements.

In the particular case of angular separation $\Theta = 90°$, the Doppler contribution vanishes. The reason is that for any 3D mode, the velocity perturbation vanishes for directions in the plane. This also applies to the contribution from our own velocity, the kinematic dipole. Thus the particular case of equatorial azimuthal symmetry (equation (8)) is particularly robust: a reconstruction is not necessary, and the symmetry survives in the temperature. An exact global equatorial symmetry of curvature (equation (8)) *implies exactly vanishing temperature correlation at 90 degrees*:

$$C_T(90°) = C_{\Delta}(90°) = 0. \tag{18}$$

This exact property of the correlation function applies even at high angular resolution in a holographic model with the exact symmetry given by equation (7); it can occur by chance in some realizations of a conventional cosmology, but only very rarely to a very high precision.

Causal constraints on correlation of polar and azimuthal information (figure 5) could also lead to exact symmetries at other angles, for example at $30°$ (equation (9)), but in this case, a reconstruction is necessary; the exact symmetry does not survive in δT.

The distribution on the sky is often described in terms of spherical harmonics $A_{\ell m}$. The angular power spectrum

$$C_\ell = \frac{1}{2\ell + 1} \sum_{m=-\ell}^{m=+\ell} |A_{\ell m}|^2 \tag{19}$$

has the same information as the angular correlation function; contributions of odd and even spherical harmonics to the correlation function are given by the standard formula (e.g., [4, 34, 35])

$$C(\Theta) = \frac{1}{4\pi} \sum_\ell (2\ell + 1)\mathcal{C}_\ell P_\ell(\cos \Theta), \tag{20}$$

where P_ℓ are the Legendre polynomials, with the property that $P_\ell(0) = 0$ for odd ℓ, $P_\ell(0) \neq 0$ for even ℓ.

In the harmonic description, a simple exact symmetry in the angular domain, such as equation (18), appears as a conspiracy of many spherical harmonic coefficients. The conspiracy extends to high ℓ, even for symmetries at large Θ. In particular, agreement with $C(90°) = 0$ requires a sum of even mode contributions to vanish at high precision up to the map resolution ℓ, which is very unlikely if they are drawn independently from random distributions as in the standard picture.

3.2. Interpretation of well known CMB anomalies

The holographic model provides a unified physical interpretation that accounts in a general way for several long-studied features of measured CMB anisotropy at low ℓ that are statistically anomalous in the standard model [4, 8, 13, 34, 36–38]. We first summarize a proposed interpretation of some well known empirical anomalies, then suggest more sharply defined theory-motivated tests that can differentiate holographic inflation from the standard picture.

1. *Axes defined by the quadrupole and octopole are closely aligned.* The *WMAP* all-sky maps [2–4] revealed a remarkably close agreement in direction for quadrupole ($\ell = 2$) and octopole ($\ell = 3$) harmonics. The aligned direction is defined by the axis that maximizes the sum of the squares of $a_{\ell,\ell}$ and $a_{\ell,-\ell}$ spherical harmonic coefficients, that is, maximizes polar asymmetry. A variety of studies have confirmed the close alignment to be highly unlikely in the standard model [34]. In our model, as discussed above, the principal axes of harmonics have to be aligned to satisfy the constraints imposed by a holographic information deficit with rotational symmetry, such as constant variance on great circles (equation (11)). Note that the alignments depend on the $A_{\ell m}$'s but not the C_ℓ's, so this is a higher-order symmetry not captured by symmetries of $C(\Theta)$.

Since the alignment axis is associated with physical primordial modes in three dimensions, whose orientation is correlated on different scales, the model could account for why 'secondary' integrated Sachs–Wolfe (ISW [29–31]) contributions from gravitational effects in the intervening volume do not spoil the precise alignment.

2. *The two-point temperature correlation function is small at large angular separation* [8, 13, 34]. An unexpected lack of large angle correlation power has been apparent since the first measurements with COBE [35].

In the *WMAP* analysis of $C(\Theta)$, based on 7 years of data [4], the authors comment on the (true) fact that there is no significant conflict with the standard random-phase scenario, and no significant deficit of large-scale power: '$C(\Theta)$ lies within the 95% confidence range of the

best-fit Λ CDM model for all Θ, as determined by Monte Carlo simulations. This supports the conclusion that there is no statistically significant lack of large-scale power on the full sky.' At the same time, compared with a standard ensemble of random-phase CMB realizations, $C(\Theta)$ is both anomalously close to zero around 90 degrees, and anomalously negative near 180 degrees.

By contrast, the published *WMAP* plot of $C_T(\Theta)$ appears to agree remarkably well with the simple and exact global equatorial symmetry (equation (18)) of holographic inflation: the measured $C_T(\Theta)$ appears to have a value at 90 degrees consistent with zero.

3. *The quadrupole and other even harmonics are smaller than expected.* As discussed above, an excess of odd over even fluctuation power [8, 13, 34], measured in harmonic decomposition, shows significant anomalous antipodal anticorrelation on angular scales much smaller than the dipole, which also appears as a significant negative correlation in $C_T(\Theta)$ near 180 degrees. Both are interpreted here as direct signatures of antipodal anticorrelation on the horizon, with $\mathcal{E} < 1$ over a wide range of ℓ (equation (16)).

3.3. New tests

In holographic inflation, precision tests of symmetries are possible on large angular scales without the usual cosmic-variance penalty on significance: predictions for symmetries are not influenced by the random variables of realizations as they are in the standard scenario. This feature allows for powerful parameter-free comparisons with standard theory.

3.3.1. Global azimuthal symmetries. The exact value of $C(\Theta)$ has no particular significance in the standard scenario, so a very close agreement with zero can indicate a likelihood with a strong preference for the holographic theory. Such a precise null test of equatorial symmetry (equation (18)) will require more attention to specific biases of foreground subtraction and masking than needed in large scale tests of the standard picture, whose predictions have a large scatter from cosmic variance.

Published *WMAP* and *Planck* plots disagree in detail. In the case of the *WMAP* ILC all-sky map [4], $C_T(90°)$ appears to be consistent with zero. In the case of *Planck* [8, 13], four different foreground removal techniques agree with each other, and $C_T(90°)$ differs slightly but significantly from zero in all of them. Recently, these maps were re-analyzed ([39]) with uniform masking. The result of this analysis was that the least biased measurements of $C(\Theta)$ from the two satellites and most of the different foreground removal techniques are in good agreement with each other near $\Theta = 90°$, and fall into a remarkably narrow range around $C(90°) = 0$. A new, more precise likelihood comparison with standard theory should be possible with closer attention to foregrounds, and with a reconstruction of C_Δ, perhaps including polarization data [32, 33].

3.3.2. Intrinsic dipole. In emergent cosmology, it is plausible that (unlike the standard scenario) there is a vanishing intrinsic dipole, because enclosed matter and its bounding CMB horizon share a common causal past (see figure 2): they are bounded by the same causal diamond, whose boundary lies at the end of inflation. As the classical metric emerges from a quantum system, the cosmic rest frame defined by the sum of cosmic matter within the horizon (that is, into which its geometrical position state collapses) should be the same as the frame defined by the bounding horizon.

This symmetry is testable in principle. The intrinsic dipole can be estimated by measuring and subtracting the contribution from galaxy flows on very large scales (> 200Mpc) that account for the dipole contributed by peculiar velocity. If the intrinsic dipole vanishes, the prediction is that the motional dipole agrees with the sky dipole. Because the first order dipole

induced by motion is so much larger than even the standard expected primordial curvature-induced intrinsic dipole, a precision test is difficult in practice: it requires a comprehensive survey of precise cosmic distances (e.g., reference [40]).

In the case that the intrinsic dipole does not vanish, it must still 'conspire' with other odd harmonics to be consistent with great-circle-variance symmetry, as discussed above. In this case, constant great-circle variance allows another test: it should be possible to uniquely reconstruct both the axis and amplitude of the dipole from measured maps.

3.3.3. Future Holometer experiments.   Nonlocal coherent fluctuations on causal diamonds, as posited here for inflation, should also affect light propagating between massive bodies in flat space on macroscopic scales [41–46]. It has recently become possible to probe these coherent Planck scale fluctuations directly in laboratory experiments, using interferometers with signal measurement bandwidth comparable with their free spectral range.

If displacements on causal diamonds in the laboratory are governed by the same uncertainty as that used for holographic cosmological perturbations (equation (5)), a differential measurement of light paths of length L displays fractional fluctuations on timescale L/c of order

$$\langle \delta L^2 \rangle / L^2 \approx L l_{\mathrm{P}}. \tag{21}$$

They may be observable as cross correlations, with Planck scale power spectral density, between signals in interferometers [41–46]. The effect on the signal depends on the directional structure of fluctuations, and the spatial structure of the light paths.

The results of such experiments depend on symmetries of the apparatus, which control its response to coherent fluctuations of causal diamonds. It has been demonstrated experimentally that there is no such effect for some configurations of the light paths. The most sensitive published measurement [47] constrains coplanar, radial quadrupolar fluctuations to more than an order of magnitude less than the amplitude in equation (21). Current experiments are studying the possibility of purely rotational or transversal fluctuations [45]. Future experiments in different configurations, including light paths extending in three dimensions, could respond to holographically entangled fluctuations of light cones similar to that posited here for inflationary horizons. A detection of cosmological spookiness could provide both motivation and design guidance for future experiments.

4. Conclusion

The simple geometrical symmetries proposed here are examples of holographic correlations: they apply to the entire sky on all scales, and reduce the independence of perturbations in different directions. The primordial structure of curvature perturbations also survives today in three dimensional large scale structure: the structural pattern of the galaxy distribution caused by spooky entanglement should display the same exotic angular correlations as the CMB pattern [18]. The candidate symmetries of holographic correlations analyzed here are predicted to appear clearly in the CMB on large scales today largely because the last scattering surface approximates a 2-sphere, like the primordial horizon where the correlations originated. For this reason, CMB anisotropy at present provides the most direct tests of the holographic-inflation hypothesis.

Directional symmetries of emergent perturbations allow the formulation of new predictions accessible to test at large angular scales with existing data. The new correlations arise from entangled relationships at large separations (Θ of order unity in the angular domain), but also

in fine grained structural detail ($\ell \gg 1$ in the wavenumber domain)—a feature distinctly absent in the standard scenario.

An important new feature of holographic inflation is that its precise symmetries allow predictions for measurements in the angular domain with no cosmic variance, so large-angle tests can achieve unaccustomed power. It is remarkable that generic, holographically-motivated symmetries approximately account for some well-known so-called 'anomalies' of CMB anisotropy. Moreover, some new predictions are unusually specific: for example, emergent causality leads to an exact value for the angular correlation function, $C_T(90°) = 0$, that has no particular significance in the standard picture. These predictions motivate new, specifically targeted combined analyses of the *WMAP* and *Planck* data, as well as new measurements of polarization over a large fraction of the sky, that can further reduce systematic errors from astrophysical foregrounds.

Precise confirmation of these emergent symmetries would lend support to the hypothesis that primordial scalar curvature perturbations originate mainly from holographically coherent quantum gravity, rather than a conventional system of quantum fields with linearized gravity. The observed perturbation pattern in that case is then a direct relic of the deeper quantum system, and its symmetries can be used to constrain theories of emergent space-time.

Acknowledgments

Appendix

A. Theoretical motivation for a coherent quantum inflationary horizon

The main hypothesis of holographic inflation is that the boundary between classical and quantum descriptions of geometry is a null surface. This long-known concept [48] allows a covariant reduction of quantum geometrical states to connect consistently with standard non-dynamical 'spooky' spacelike quantum relationships among particle states [49–51]. Standard quantum inflation adopts a model quantum system based on effective field theory and linearized gravity, and does not have this property: its decomposition into comoving waves is motivated by linear evolution equations based on continuous derivatives, which depend on classical locality. It is useful to summarize some current threads of gravitational theory that motivate the holographic model.

In an explicit quantum model of eternal black holes that includes gravitational back-reaction by emission and absorption of quantum particles [19–21], the horizon of a black hole is a coherent quantum object, so that a measurement by an external observer nonlocally affects its global state. This hypothesis allows an elegant solution of many paradoxes associated with quantum black holes (e.g., [52–55]). The calculation has been extrapolated to causal diamonds in flat space-time, where it leads to directionally coherent macroscopic fluctuations [46]. The main assumption of the current work is that the inflationary horizon has a similar global coherence.

Another powerful line of argument is based on a derivation of Einstein's field equations [56, 57] from the requirement that any patch of a null surface behaves like a black hole horizon, in the accelerating frame where it is the observer's horizon. This result supports the view that

classical space-time and gravitation are emergent, collective quantum phenomena [56–59], and that holographic and thermodynamic properties of black hole horizons generalize to universal properties of null surfaces in any space-time [60–62]. In holographic inflation, the horizon is taken to be the light cone that bounds the past of an observer at the end of inflation; coherent fluctuations of its nested causal diamonds freeze in as classical potentials when other comoving locations pass through it.

Coherent properties of geometrical states have also been extensively studied in anti-de Sitter space [63–65]. In this case, nonlocal spacelike correlations are encoded in a dual theory, that of a conformal field on the lower-dimensional boundary.

B. Estimates of coherent fluctuations of causal diamonds and horizons from a semiclassical correspondence principle

In spite of considerable theoretical attention recently to the mathematical nature of nonlocalized information in black holes [66–68], there is as yet no consensus on the magnitude or physical effects of coherent, large-angle fluctuations of horizons [22, 23] or causal diamond surfaces [46].

Here, we estimate the magnitude and nonlocal coherence of physical effects from Planck scale quantum gravity, using the Bohr correspondence principle for some simple systems. In this view, the quantum system is a 'sum over histories', or a superposition of different metrics, without presuming that these states decompose into independent plane-wave perturbations. Instead, the macroscopic effect of a quantum system is required to match its classical behavior, so that the active gravity of a quantum system of particles can have the same coherence as the particle state. These simple examples show how such coherence amplifies the effect of Planck scale fluctuations on large scales, and entangles causal structure in different directions. They indicate that the dominant quantum fluctuations of coherent causal diamonds or horizons of any size R come from the Planck scale, rather than fluctuations of a field vacuum modes of wavelength R.

B.1. Gravitational shock waves of point particles with Planck momentum in flat space-time.

Consider the classical gravitational effect of a null point particle [19–21, 69, 70], as shown in figure B1. A localized pointlike momentum impulse p with impact parameter $x_\perp$ creates an invariant coherent delocalized transverse displacement everywhere on a light sheet,

$$\delta u = 4Gp \ln(x_\perp^2). \tag{22}$$

This displacement represents a real, physical distortion of causal structure; the motion of matter 'drags' the space-time along with it.

Now consider the gravitational effect of a quantum state: a pair of Planck momentum particles emitted in a spherical wave function, like a pair of antipodally propagating gamma rays from annihilations in a PET imager. For any given emission axis, the shocks create a uniform inwards displacement of the surface everywhere on the equator of the axis determined by a particle pair, as shown on the right side of figure 6. Since the axis is indeterminate until the particle wave collapses, the gravitational state must have the same geometrical coherence. Thus, after a duration τ the correspondence principle requires coherent nonlocal correlations of displacement δu everywhere on a causal diamond surface of size $c\tau$, for consistency of GR with any axis of the particle pair. The magnitude of displacement is independent of the size of the diamond.

The same correlations between poles and equator apply for a random sequence of impulses in different directions. The distortion of causal structure is additive after each shock wave

passes, so the amplitude from many pairs does not cancel, but adds in quadrature. For Planck-momentum fluctuations every Planck time (the scale of fluctuations in models with discrete time at the Planck scale [71]), the sum after time τ is

$$\langle \Delta^2 \rangle \sim t_\text{P}/\tau. \tag{23}$$

This estimate agrees with previous estimates based on random walks of world lines, standard quantum uncertainty and wave diffraction [44, 72, 73]. This set-up explicitly shows the coherent separation between radial and transverse (angular) degrees of freedom, and the unattenuated macroscopic transverse effects of Planck scale particles on an arbitrarily large scale. These coherent properties of classical particles should also apply to the gravitational effect of their quantum states; the causal structure needs to inherit the same spooky, transverse correlations.

We have invoked a similar amplitude and transverse coherence for the inflationary horizon. In the inflationary system, null trajectories curve and in general acquire transverse components, leading to the angular-domain correlations. The flat-space gravitational shock wave shows the magnitude of the coherent Planck scale fluctuation that might appear in experimental signals, but does not include the process of freezing on the horizon.

B.2. Classical tides from point masses added and subtracted from a black hole. The back-reaction of quantum point particles entering and leaving a black hole horizon, including antipodal correlations, was studied in refs. [19–21], with the gravitational effect based on the gravitational shock wave in the Rindler frame. Here, we use classical correspondence to estimate the tidal distortion of the shape of the black hole horizon by point particles.

A point mass falling into a black hole of radius R raises a tide and creates a coherent distortion of the horizon with a significant quadrupolar component on a timescale c/R. For addition of many point masses in a time $< R/c$, the mean square quadrupole amplitude adds in quadrature. For each mass m, $\delta R/R \sim m/M$, so N of them produce $\langle (\delta R/R)^2 \rangle \sim N(m/M)^2$.

Quantum horizons should have similar coherence. Suppose again (e.g., as in [71]) that there is some form of discreteness in proper time at the Planck scale. Suppose that each Planck time, a Planck mass particle fluctuates in or out of the hole. Their mean contributions average out, but for random orientations, their large-angle, low-multipole distortions add in quadrature. In this case, $N \sim R/ct_\text{P}$, so the the variance of the horizon distortion is given by $\langle \Delta^2 \rangle = \langle h^2 \rangle = \langle \delta R^2 \rangle/R^2 \sim ct_\text{P}/R$, again the same as the estimate used for holographic horizon. The states are similarly nonlocally entangled over a time $\sim R/c$ like a coherent quantum spin state, creating a superposition and entanglement of directions.

B.3. Virtual quadrupolar distortion of a black hole necessary to radiate classically at the Hawking rate. In linear gravity, a source emits gravitational radiation according to the standard classical quadrupole formula,

$$h_\text{wave} = (G/r)\ddot{I}_{ij}, \tag{24}$$

where h_wave is strain of the wave at distance r, and $I_{ij} = \int \text{d}^3 x \rho x_i x_j$ represents the quadrupole of the matter distribution. For coherent quadrupolar vibrational distortions of a black hole horizon of magnitude

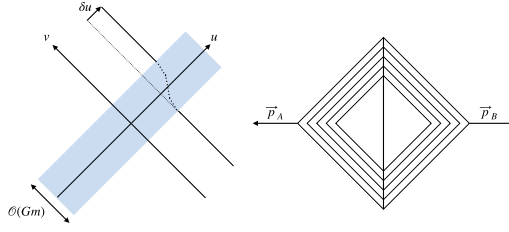$$h_\text{horizon} \sim \delta R/R, \tag{25}$$

we have approximately

Figure B1. Classical gravitational shocks in nearly-flat space-time from a point mass m, adapted from reference [69]. In null coordinates u, v, the displacement δu due to gravitational drag (equation (22)) is shown as a function of v for a point particle moving in the u direction with momentum $p \gg mc$. The physical displacement is axially symmetric around the particle trajectory and independent of the impact parameter of the particle, $x_\perp$. At right, the spatial patterns of shock waves from counterpropagating particles are shown.

$$\ddot{I}_{ij} \sim h_{\text{horizon}}^2 (R/G). \tag{26}$$

Thus,

$$h_{\text{wave}} \sim h_{\text{horizon}}^2 (R/r), \tag{27}$$

so in the near-wave zone with $R \sim r$,

$$h_{\text{wave}} \sim h_{\text{horizon}}^2. \tag{28}$$

That is, in the classical system, gravitational waves are second order compared to the distortions of causal structure that generate them.

In the semiclassical, sum-over-histories view, the virtual metric fluctuations of a quantum black hole horizon in the near field are also much larger than the metric fluctuations of the Hawking radiation that escapes from the system and carries energy away. The power per area of a classical localized gravitational-wave packet, comparable in size to wavelength $\sim 2\pi c/\omega$ in all directions, is about $\sim \langle h_{\text{wave}}^2 \rangle c^3 \omega^2 / G$; the metric of strain of a single graviton wave packet localized to the same volume is

$$\langle h_{\text{wave}}^2 \rangle \sim (t_{\text{P}}\omega)^2. \tag{29}$$

The typical equivalent classical strain of Hawking radiation from a black hole of size $R \sim c/\omega$ on the scale $r \sim R$ as it leaves the vicinity of the hole is $\langle h_{\text{wave}}^2 \rangle \sim (ct_{\text{P}}/R)^2$; the horizons in the quantum superposition vary coherently with quadrupole amplitude

$$\langle h_{\text{horizon}}^2 \rangle \sim (ct_{\text{P}}/R). \tag{30}$$

The Hawking radiation can be viewed as an atom-like transition between these states.

During inflation, the equivalent of h_{wave} is the metric strain of tensor modes generated by quantum fluctuations [74] on the horizon scale, the zero point oscillations of a field mode of frequency $\omega = H$. In holographic inflation, the scalar perturbations arise from coherent Planck scale fluctuations in the locations (or equivalently, clocks) of world lines on the scale $R = c/H$, not zero point of field modes of frequency H. Thus, as in the classical black hole,

$$\langle h_{\text{horizon}}^2 \rangle \sim \langle h_{\text{wave}}^2 \rangle^{1/2} \sim H t_{\text{P}} \tag{31}$$

so scalar perturbations are much larger than the tensor distortions, which have $\langle h_{\text{T}}^2 \rangle = (H t_{\text{P}})^2 / 2\pi^2$.

C. Spin-algebra model of coherent quantum causal diamond fluctuations in flat space-time

The physical consequences of geometrical nonlocality depend on the connection of quantum mechanics and space-time at a basic level. If geometry and locality are emergent properties of a quantum system, the quantum-field approximation to the system breaks down, as it omits important entanglements between matter and geometrical degrees of freedom.

This section develops a covariant model of emergent, coherent quantum causal diamond states in a flat background. It provides a concretely defined quantum system to illustrate physical effects of a new form of nonlocal geometrical entanglement, not included in standard quantized linear gravity. This model does not address quantum dynamics at the Planck scale, nor is it a substitute for other, arguably more fundamental theories of quantum gravity [75–77]. It is introduced to reveal measurable physical effects of coherent causal diamond states that differ from effective field theory and linearized gravity: the large fluctuations introduced by coherence, and new symmetries of transverse or directional correlations. These effects are found in a regime not easily accessible in other approaches, on scales much larger than $c t_{\text{P}}$.

C.1. Dirac light cone function.
Locality on light cones is conventionally defined by the covariant four-dimensional generalization of the one-dimensional Dirac δ-function (reference [78], section 75):

$$\Delta(x) = 2\delta(x^\mu x_\mu) x_0 / |x_0|, \tag{32}$$

where $x_\mu = (t, \vec{r})$ represents 4-position. It vanishes at the origin, and is nonvanishing on past and future light cones from the origin. It is odd in timelike directions and even at spacelike separations, with a 4D point-parity antisymmetry that combines time and space,

$$\Delta(-x) = -\Delta(x). \tag{33}$$

It has a purely imaginary transform, of the same functional form,

$$\tilde{\Delta}(k) \equiv \int \mathrm{d}^4 x \Delta(x) \mathrm{e}^{ikx} = 4\pi^2 i \Delta(k). \tag{34}$$

C.2. Locality of quantum field states.
The standard model of locality for field states is based on point localization in a classical space-time background. To quantize fields [78, 79], the light cone function is used to write covariant commutation relations for field operators $\hat{A}(x)$,

$$[\hat{A}_\mu(x), \hat{A}_\nu(x')] = g_{\mu\nu} \Delta(x - x'), \tag{35}$$

where $g_{\mu\nu}$ denotes a (classical) tensor. The explicit geometrical coefficients on the right-hand side are all classical objects: geometry is not part of the quantum system. There is an unwritten quantum operator on the right side which is just the identity operator on a field state. Since the only position dependence on the right side comes in classical functions, there is no entanglement of field states with geometry.

For field dynamics, it is necessary to include conjugate momentum or derivative operators. This leads to propagating states in the form of plane waves, with a commutator for the transform of quantized wave modes

$$[\hat{A}_\mu(\vec{k}), \hat{A}_\nu(\vec{k}')] = ig_{\mu\nu}\delta(\vec{k} - \vec{k}')/4\pi^2 k_0, \tag{36}$$

where $g_{\mu\nu}$ again denotes a (classical) tensor. The coefficient depends on the spin or helicity of the field, and relates internal quantum degrees of freedom to the classical inertial frame. In the case of linearized gravity the propagating quanta are gravitons, a spin 2 tensor field with a very small self coupling set by the Planck scale.

In standard inflation, perturbations arise from linearized gravity coupled to quantum fluctuations of field vacuum states. The 'collapse' of these states into a classical metric occurs coherently in $\vec{k}$ space, for each spatially infinite mode. In holographic or spooky inflation, these perturbations are subdominant to those from new fundamental geometrical quantum degrees of freedom that underlie holographic, emergent gravity [17, 18].

C.3. Model of coherent causal diamond fluctuations. A simple model of a geometrical quantum system can be built from new geometrical operators $\hat{\tau}_\kappa$, whose fluctuations will ultimately be identified as perturbations in potential. A contraction with the antisymmetric Levi-Civita 4-tensor $\epsilon_{\kappa\lambda\mu\nu}$ allows us to write a Lorentz covariant generalized rotational commutative algebra with the same light cone structure as the field commutator (equation (35)):

$$[\hat{\tau}_\kappa, \hat{\tau}_\lambda] = i\epsilon_{\kappa\lambda\mu\nu}\,\hat{\tau}^\mu\,\Delta(x^\nu)\tau_0. \tag{37}$$

The imaginary coefficient in equation (37) allows for superposition and entanglement of the geometrical states. In equation (37), geometrical quantum operators on both sides share the same degrees of freedom, so there are new nonlocal quantum relations that cannot be described by equation (35), even with a linearized tensor field to represent quantum gravity.

Equation (37) is not a fully consistent noncommutative quantum geometry, since the light cone function $\Delta(x^\nu)$ is not a quantum operator and a classical metric has been used for raising and lowering the indices. It projects the geometrical state onto a classical metric, and the operator labels onto a classical inertial frame. In the physical interpretation below, the classical metric corresponds to a measurement, and thereby a choice of observer world line and inertial frame.

The localization scale τ_0 has the same dimensions as $\hat{\tau}$. It fixes the information content of the system in physical units. In our physical interpretation of this system, $\Delta(x^\nu)$ is a function of physical space-time event positions, so τ_0 represents a quantization scale of light cone states in the frame of an emergent observer—a finite resolution in proper time. As shown below, for a system that obeys the holographic principle, such as emergent gravity, $\tau_0 = t_P$. This Planck-scale normalization will be assumed in the following.

C.4. Nonlocal information, projection and uncertainty. Even though the degrees of freedom represented by the $\hat{\tau}_\kappa$'s have no local or dynamical effects, their fluctuations in time and direction affect correlations in nonlocal measurements.

Consider projection onto a 3D spacelike surface of constant $x^0 \neq 0$. The light cone function $\Delta(x_0)$ is then a δ-function on a 2-sphere of radius $|x_0|$, which coincides with the surface of a causal diamond. For spatial positions on this surface, we can set $\nu = 0$ in equation (37) to obtain a standard spin algebra in three dimensions, with relabeled indices i, j, k taking values $1, 2, 3$,

$$[\hat{\tau}_i, \hat{\tau}_j] = i\epsilon_{ijk}\hat{\tau}_k t_P. \tag{38}$$

21

Thus, when a light cone function $\Delta(x^\nu)$ is used to project the four dimensional space-time operators onto three dimensions—an eigenstate of proper time—it creates a fully consistent quantum algebra that entangles curvature fluctuations in three dimensions.

We now recall some standard results of quantum mechanical spin in three dimensions (e.g., [80, 81]). Positions in each spatial direction are related by

$$[\hat\tau_1, \hat\tau_2] = i\hat\tau_3 t_P, \tag{39}$$

and its cyclic permutations. A radial operator $\hat\tau^2 \equiv \sum \hat\tau_i^2$ commutes with all direction components:

$$[\hat\tau_i, \hat\tau^2] = 0. \tag{40}$$

The discrete states of the system are assembled using raising and lowering operators. For direction 3,

$$\hat\tau_{3\pm} = \hat\tau_1 \pm i\hat\tau_2 \tag{41}$$

with the commuting properties

$$[\hat\tau_3, \hat\tau_{3\pm}] = \pm t_P \hat\tau_{3\pm}, \tag{42}$$

with raising and lowering operators for the other directions again obtained by cyclical permutations of $1, 2, 3$. In a conventional integer-spin representation, $l = 0, 1, 3, \ldots,$ denotes the principal quantum number, and $m = -l \cdots + l$ denotes projections onto a chosen axis, say 3. The eigenvalues of $\hat\tau^2$ are $l(l+1)t_P^2$, and the eigenvalues of $\hat\tau_3$ are $m_l t_P$.

For each l there are $2l + 1$ directional projection eigenstates, so the number of degrees of freedom $\mathcal{N}$ scales holographically, as the surface area in Planck units:

$$\mathcal{N} = \sum_{l'=0}^{l} (2l' + 1) \approx (|\tau|/t_P)^2, \tag{43}$$

where the approximation applies in the large l limit. Thus, a Planck scale normalization agrees with holographic emergent gravity [56–59]. We interpret $\mathcal{N}$ as the geometrical information in the whole (3+1D) volume enclosed by a (2+1D) causal diamond defined by a 1D proper time interval.

Using standard algebraic methods [18, 80, 81], it can be shown that in an eigenstate of $\hat\tau_3$,

$$\langle \hat\tau_1 \rangle = \langle \hat\tau_2 \rangle = 0 \tag{44}$$

and

$$\langle \hat\tau_1^2 \rangle = \langle \hat\tau_2^2 \rangle = \langle \hat\tau^2 - \hat\tau_3^2 \rangle/2 = t_P^2[l(l+1) - m^2]/2. \tag{45}$$

Since $m^2 \leqslant l^2$, we can write a generalized uncertainty principle for quantum fluctuations in any three orthogonal directions:

$$\langle \delta\tau^2 \rangle \equiv \langle \delta\hat\tau_1^2 \rangle + \langle \delta\hat\tau_2^2 \rangle + \langle \delta\hat\tau_3^2 \rangle \geqslant l\, t_P^2 > |\tau| t_P, \tag{46}$$

where

$$\delta\hat\tau_i^2 \equiv \langle \hat\tau_i^2 \rangle - \langle \hat\tau_i \rangle^2. \tag{47}$$

For large l, the uncertainty (equation (46)) is much larger than t_P^2. In our interpretation of this system, the $\delta\hat{\tau}_i$'s represent fluctuations in time as function of direction on causal diamond surface of fixed radius, so the fractional fluctuations

$$\langle \delta\tau^2 \rangle / |\tau|^2 = t_P/|\tau| \tag{48}$$

represent perturbations in gravitational redshift, dimensionless potential or curvature as a function of direction on a surface of radius $c|\tau|$. A causal diamond in flat space-time, or a horizon during inflation, has a 2D bounding surface radius with coherent quantum fluctuations of this magnitude (as in Equation (5)), nonlocally entangled among all three directions.

ORCID iDs

Craig Hogan ⓘ https://orcid.org/0000-0002-1433-8841

Reference

[1] Weinberg S 2008 *Cosmology* (Oxford: Oxford University Press)

[2] Bennett C L *et al* 2013 Nine-year Wilkinson microwave anisotropy probe (WMAP) observations: final maps and results *Astrophys. J. Suppl. Ser.* **208** 20

[3] Hinshaw G *et al* 2013 Nine-year Wilkinson microwave anisotropy probe (WMAP) observations: cosmological parameter results *Astrophys. J. Suppl. Ser.* **208** 19

[4] Bennett C L *et al* 2011 Seven-year Wilkinson microwave anisotropy probe (wmap) observations: are there cosmic microwave background anomalies? *Astrophys. J. Suppl. Ser.* **192** 17

[5] Ade P A R *et al* 2016 Planck 2015 results. XIII. Cosmological parameters *Astron. Astrophys.* **594** A13

[6] Ade P A R *et al* 2016 Planck 2015 results. XX. Constraints on inflation *Astron. Astrophys.* **594** A20

[7] Ade P A R *et al* 2016 BICEP2, Keck Array improved constraints on cosmology and foregrounds from BICEP2 and Keck Array cosmic microwave background data with inclusion of 95 GHz band *Phys. Rev. Lett.* **116** 031302

[8] Ade P A R *et al* 2016 Planck 2015 results. XVI. Isotropy and statistics of the CMB *Astron. Astrophys.* **594** A16

[9] Aylor K *et al* SPT 2017 A comparison of cosmological parameters determined from CMB temperature power spectra from the south pole telescope and the Planck satellite *Astrophys. J.* **850** 101

[10] Akrami Y *et al* 2019 Planck 2018 results. I. Overview and the cosmological legacy of Planck *Astron. Astrophys.* (accepted) https://doi.org/10.1051/0004-6361/201833880

[11] Aghanim N *et al* 2018 Planck 2018 results. VI. Cosmological parameters (arXiv:1807.06209 [astro-ph.CO])

[12] Akrami Y *et al* 2019 Planck 2018 results. X. Constraints on inflation *Astron. Astrophys.* (accepted) https://doi.org/10.1051/0004-6361/201833887

[13] Akrami Y *et al* 2019 Planck 2018 results. VII. Isotropy and statistics of the CMB *Astron. Astrophys.* (accepted) https://doi.org/10.1051/0004-6361/201935201

[14] Kadota K, Scott D, Hu W and Stewart E D 2005 Stewart precision of inflation potential reconstruction from CMB using the general slow-roll approximation *Phys. Rev.* D **72** 023510

[15] Baumann D 2011 Inflation *Physics of the Large and the Small* (TASI 09) ed C Csaki (Singapore: World Scientific) pp 523–686

[16] Kamionkowski M and Kovetz E V 2016 The quest for B Modes from inflationary gravitational waves *Ann. Rev. Astron. Astrophys.* **54** 227–69

[17] Banks T and Fischler W 2018 The holographic spacetime model of cosmology *Int. J. Mod. Phys.* D **27** 1846005

[18] Hogan C 2019 Nonlocal entanglement and directional correlations of primordial perturbations on the inflationary horizon *Phys. Rev.* D **99** 063531

[19] Hooft G t 2016 The quantum black hole as a hydrogen atom: microstates without strings attached (arXiv:1605.05119 [gr-qc])

[20] Hooft G 't 2016 Black hole unitarity and antipodal entanglement *Found. Phys.* **46** 1185–98

[21] Hooft G t 2018 Virtual black holes and space-time structure *Found. Phys.* **48** 1134–49

[22] Giddings S B 2019 Quantum-first gravity *Found. Phys.* **49** 177–90

[23] Giddings S B 2019 Black holes in the quantum universe *Proc., Topological Avatars of New Physics* (London, United Kingdom March 4–5, 2019) Phil. Trans. Roy. Soc. Lond. A **377** 20190029

[24] Hogan C J 2002 Holographic discreteness of inflationary perturbations *Phys. Rev.* D **66** 023521

[25] Hogan C J 2004 Discrete spectrum of inflationary fluctuations *Phys. Rev.* D **70** 083521

[26] Hogan C J 2002 Observing the beginning of time: new maps of the cosmic background radiation may display evidence of the quantum origin of space and time *Am. Sci.* **90** 420–7

[27] Scardigli F, Gruber C and Chen P 2011 Black hole remnants in the early universe *Phys. Rev.* D **83** 063507

[28] Bardeen J M 1980 Gauge-invariant cosmological perturbations *Phys. Rev.* D **22** 1882–905

[29] Sachs R K and Wolfe A M 1967 Perturbations of a cosmological model and angular variations of the microwave background *Astrophys. J.* **147** 73

[30] Hu W and Scott D 2002 Cosmic microwave background anisotropies *Annu. Rev. Astron. Astrophys.* **40** 171–216

[31] Wright E 2003 Theoretical overview of cosmic microwave background anisotropy *Measuring and Modeling the Universe Proc. Symp.* (Pasadena, USA November 17–22, 2002) pp 291–308 (arXiv:astro-ph/0305591 [astro-ph])

[32] Yadav A P and Wandelt B D 2005 CMB tomography: Reconstruction of adiabatic primordial scalar potential using temperature and polarization maps *Phys. Rev.* D **71** 123004

[33] Dorn S, Greiner M and En A T 2015 All-sky reconstruction of the primordial scalar potential from WMAP temperature data *J. Cosmol. Astropart. Phys.* JCAP02(2015)041

[34] Schwarz D J, Copi C J, Huterer D and Starkman G D 2016 CMB anomalies after Planck *Class. Quant. Grav.* **33** 184001

[35] Hinshaw G, Banday A J, Bennett C L, Górski K M, Kogut A, Lineweaver C H, Smoot G F and Wright E L 1996 Two-point correlations in the [ITAL]COBE[/ITAL] DMR four-year anisotropy maps *Astrophys. J.* **464** L25–L28

[36] Aluri P K, Ralston J P and Weltman A 2017 Alignments of parity even/odd-only multipoles in CMB *Mon. Not. R. Astron. Soc.* **472** 2410–21

[37] Aluri P K and Jain P 2012 Parity asymmetry in the CMBR temperature power spectrum *Mon. Not. R. Astron. Soc.* **419** 3378–92

[38] Copi C J, Huterer D, Schwarz D J and Starkman G D 2015 Large-scale alignments from WMAP and Planck *Mon. Not. R. Astron. Soc.* **449** 3458–70

[39] Hagimoto R, Hogan C, Lewin C and Meyer S S 2020 Symmetries of CMB temperature correlation at large angular separations *Astrophys. J.* **888** L29

[40] Qin F, Howlett C, Staveley-Smith L and Tao H 2018 Bulk flow in the combined 2MTF and 6dFGSv surveys *Mon. Not. Roy. Astron. Soc.* **477** 5150–66

[41] Hogan C J 2012 Interferometers as probes of Planckian quantum geometry *Phys. Rev.* D**85** 064007

[42] Kwon O and Hogan C J 2016 Interferometric tests of Planckian quantum geometry Models *Class. Quantum Grav.* **33** 105004

[43] Hogan C J and Kwon O 2017 Statistical measures of planck scale signal correlations in interferometers *Class. Quantum Grav.* **34** 075006

[44] Hogan C J 2017 Exotic rotational correlations in quantum geometry *Phys. Rev.* D **95** 104050

[45] Hogan C J, Kwon O and Richardson J 2017 Statistical model of exotic rotational correlations in emergent space-time *Class Quantum Grav* **34** 135006

[46] Verlinde E P and Zurek K M 2019 Observational signatures of quantum gravity in interferometers (arXiv:1902.08207 [gr-qc])

[47] Chou A *et al* 2017 Holometer Collaboration Interferometric constraints on quantum geometrical shear noise correlations *Class. Quant. Grav.* **34** 165005

[48] Wheeler J A 1946 Problems and prospects in elementary particle research *Proc. Am. Phil. Soc.* **90** 36–47

[49] Zeilinger A 1999 Experiment and the foundations of quantum physics *Rev. Mod. Phys.* **71** S288–97

[50] Rovelli C 1991 What is observable in classical and quantum gravity? *Class. Quantum Grav.* **8** 297–316

[51] Pikovski I, Zych M, Costa F and Brukner Č 2017 Time dilation in quantum systems and decoherence *New J. Phys.* **19** 025011

[52] Unruh W G and Wald R M 2017 Information loss *Rep. Prog. Phys.* **80** 092002

[53] Cohen A G, Kaplan D B and Nelson A E 1999 Effective field theory, black holes, and the cosmological constant *Phys. Rev. Lett.* **82** 4971

[54] Solodukhin S N 2011 Entanglement entropy of black holes *Living Rev. Rel.* **14** 8

[55] Carney D, Stamp P C E and Taylor J M 2019 "Tabletop experiments for quantum gravity: a user's manual *Class. Quantum Grav.* **36** 034001

[56] Jacobson T 1995 Thermodynamics of spacetime: The Einstein equation of state *Phys. Rev. Lett.* **75** 1260

[57] Jacobson T 2016 Entanglement equilibrium and the Einstein equation *Phys. Rev. Lett.* **116** 201101

[58] Verlinde E 2011 On the origin of gravity and the laws of Newton *J. High Energy Phys.* JHEP04(2011)029

[59] Padmanabhan T 2014 General relativity from a thermodynamic perspective *Gen. Relativ. Gravit.* **46** 1673

[60] Hooft G t 1993 Dimensional reduction in quantum gravity *Conf. on Highlights of Particle and Condensed Matter Physics* (SALAMFEST) (Trieste, Italy March 8–12, 1993) Conf. Proc. C930308 pp 284–96

[61] Susskind L 1995 The world as a hologram *J. Math. Phys.* **36** 6377

[62] Bousso R 2002 The Holographic principle *Rev. Mod. Phys.* **74** 825–74

[63] Ryu S and Takayanagi T 2006 Holographic derivation of entanglement entropy from AdS/CFT *Phys. Rev. Lett.* **96** 181602

[64] Ryu S and Takayanagi T 2006 Aspects of holographic entanglement Entropy *J. High Energy Phys.* JHEP08(2006)045

[65] Natsuume M 2015 *AdS/CFT Duality User Guide* (Lect. Notes Phys.) vol 903 pp 1–294

[66] Hawking S W, Perry M J and Strominger A 2016 Soft hair on black holes *Phys. Rev. Lett.* **116** 231301

[67] Haco S, Hawking S W, Perry M J and Strominger A 2018 Black Hole Entropy and Soft Hair *J. High Energy Phys.* JHEP12(2018)098

[68] Nomura Y 2019 Spacetime and universal soft modes—black holes and beyond (arXiv:1908.05728 [hep-th])

[69] Dray T and Hooft G t 1985 The gravitational shock wave of a massless particle *Nucl. Phys.* B **253** 173–88

[70] Aichelburg P C and Sexl R U 1971 On the gravitational field of a massless particle *Gen. Relativ. Gravit.* **2** 303–12

[71] Chatwin-Davies A, Kempf A, Robert T and Martin W 2017 Natural Covariant Planck Scale Cutoffs and the Cosmic Microwave Background Spectrum *Phys. Rev. Lett.* **119** 031301

[72] Hogan C J 2008 Measurement of quantum fluctuations in geometry *Phys. Rev.* D **77** 104031

[73] Hogan C J 2008 Indeterminacy of holographic quantum geometry *Phys. Rev.* D **78** 087501

[74] Starobinsky A A 1980 A new type of isotropic cosmological models without singularity *Phys. Lett.* B **91** 99–102

[75] Polchinski J 1998 *String Theory* (Cambridge: Cambridge University Press)

[76] Schwarz J H 2000 Introduction to superstring theory (arXiv:hep-ex/0008017)

[77] Rovelli C 2004 *Quantum Gravity* (Cambridge: Cambridge University Press)

[78] Dirac P A M 1958 *Quantum Mechanics* (Oxford: Oxford University Press)

[79] Weinberg S 1996 *The Quantum Theory of Fields* (Cambridge: Cambridge University Press)

[80] Dicke R H and Wittke J P 1960 *Introduction to Quantum Mechanics* (Reading: Addison-Wesley)

[81] Landau L D and Lifshitz E M 1977 *Quantum Mechanics: Non-relativistic Theory* (Oxford: Pergamon)